PET/NIR Imaging

DOI: 10.1002/ange.201205271

Aptamer-Functionalized, Ultra-Small, Monodisperse Silica Nanoconjugates for Targeted Dual-Modal Imaging of Lymph Nodes with Metastatic Tumors**

Li Tang, Xujuan Yang, Lawrence W. Dobrucki, Isthier Chaudhury, Qian Yin, Catherine Yao, Stéphane Lezmi, William G. Helferich, Timothy M. Fan,* and Jianjun Cheng**

Metastases are responsible for 90% of human cancer deaths.[1] Most solid tumors metastasize through the circulation system, and the sentinel lymph node (LN) is typically the first site reached by the disseminating malignant cancer cells.[2] The detection of LN metastases is therefore crucial for accurate tumor staging and therapeutic decision making.[3] The current standard method for LN assessment is lymphography using a vital blue dye. However, this method is invasive, involving extended nodal dissection, and can give a false negative result if an LN is missed in surgery.[4] A non-invasive LN imaging technique is urgently needed to improve the accuracy of tumor staging.[5] Various techniques for sentinel LN imaging have been investigated, such as near-infrared (NIR) fluorescence imaging, computed tomography (CT), magnetic resonance imaging (MRI), positron emission tomography (PET), and ultrasound and photoacoustic imaging.[4b,5b,6] However, each technique has its drawbacks, and none is sufficient to provide all the necessary information for LN assessment.[4b] PET is the most sensitive and specific technique for in vivo molecular imaging,[7] but it suffers from low spatial resolution. In contrast, fluorescence imaging has high resolution and allows spatial visualization, which is helpful for intraoperative guidance; but its application is limited by poor tissue penetration. Therefore, combination of both PET and fluorescence imaging together potentially permit non-invasive assessment of LNs with high sensitivity and excellent spatial resolution.

Silica nanoparticles (NPs) are widely used for biomedical imaging applications because of the good biocompatibility and optical transparency of silica.[8] We recently developed a versatile, size-controlled, monodisperse, drug/dye silica nanoconjugate (NC) that allows for conjugation with a variety of functional moieties.[9] The robust silane chemistry and the formulation strategy permit the construction of multifunctional NCs, such as multi-modal imaging probes for in vivo applications. It is generally accepted that the physicochemical properties of NPs, especially their size, play a vital role in the systemic and lymphatic biodistribution.[10] Because the size of the silica NCs can be precisely controlled, they are ideal for investigating size effects on their trafficking behavior in the lymphatic system. The silica NCs are multifunctional and give excellent size control for the preparation of nanoparticulate probes with optimized properties for improved imaging of LN metastases.[10c]

There have been many studies on the targeting of primary tumors,[11] but very few attempts have been made to actively target metastatic tumors specifically.[12] As an alternative to antibodies for cancer targeting, aptamers, single-stranded oligonucleotides that can bind to target molecules with high specificity and affinity, have attracted much attention because they are small, easy to synthesize, non-immunogenic, and can be modified to resist denaturation and biodegradation.[13] The capability of aptamers to target primary tumors has been demonstrated in several studies in vivo.[13b,c] However, active targeting of lymphatic metastases using aptamers has not been reported.

Herein, we report a convenient, one-pot synthesis of monodisperse, size-controlled silica NC probes for dual-modal LN imaging using PET and NIR fluorescence. Monodisperse 20 nm silica NCs accumulated in sentinel LNs more rapidly and to a greater extent than larger NCs (200 nm) and were superior for efficient LN imaging. To further enhance the targeting of LNs with metastatic tumors, we functionalized the 20 nm silica NCs with a 26-mer G-rich DNA aptamer (Apt) derived from AS1411, which has high binding affinity for nucleolin (NCL), a protein that is over-expressed in the cytoplasm and on the plasma membrane of some cancer cells, including breast cancer cells.[14] The NCL-Apt-functionalized silica NCs showed markedly enhanced uptake in LNs with metastatic tumors in a murine breast tumor model, and

[*] L. Tang, I. Chaudhury, Q. Yin, C. Yao, Prof. Dr. J. Cheng
Department of Materials Science and Engineering,
University of Illinois at Urbana-Champaign
1304 W. Green Street, Urbana, IL, 61801 (USA)
E-mail: jianjunc@illinois.edu
Dr. X. Yang, Prof. Dr. W. G. Helferich
Department of Food Science and Human Nutrition (USA)
E-mail: helferic@illinois.edu
Prof. Dr. L. W. Dobrucki
Department of Bioengineering (USA)
Prof. Dr. S. Lezmi
Department of Pathobiology (USA)
Prof. Dr. T. M. Fan
Department of Veterinary Clinical Medicine (USA)
E-mail: t-fan@illinois.edu

[**] J.C. acknowledges support from the NIH (Director's New Innovator Award 1DP2OD007246-01 and 1R21CA152627). L.T. was funded at University of Illinois at Urbana-Champaign from NIH National Cancer Institute Alliance for Nanotechnology in Cancer "Midwest Cancer Nanotechnology Training Center" Grant R25 CA154015A.

Supporting information for this article (experimental details) is available on the WWW under http://dx.doi.org/10.1002/anie.201205271.

improved the detection efficiency of metastatic tumors in LNs.

Silica NCs for dual-modal imaging were synthesized in a manner similar to that reported recently.[9] We first synthesized a silane-modified NIR dye (NIR-sil) and a silanized chelating reagent (DOTA-sil) that can bind a radionuclide (e.g., ^{64}Cu) for PET imaging. Because silica is optically transparent and its excitation and emission wavelengths can pass through the silica matrix, NIR-sil was added immediately after the addition of tetraethyl orthosilicate (TEOS) so that the NIR-imaging ligand was stably bound to and homogeneously distributed in the silica NCs (Scheme 1).[8b,15] DOTA-sil was added to the NIR-dye-doped silica NCs for conjugation of DOTA to their surface for chelation of radionuclides. Poly(ethylene glycol)-containing silane (PEG-sil) was then used to conjugate PEG to the surface of the silica NCs. Surface PEGylation of NPs is routinely employed to prolong circulation, minimize nonspecific absorption, and reduce particle aggregation in vivo.[16] Finally, the as-prepared PEGylated NCs were labeled with ^{64}Cu, by means of a chelation reaction (Scheme 1; Supporting Information, Figure S1).

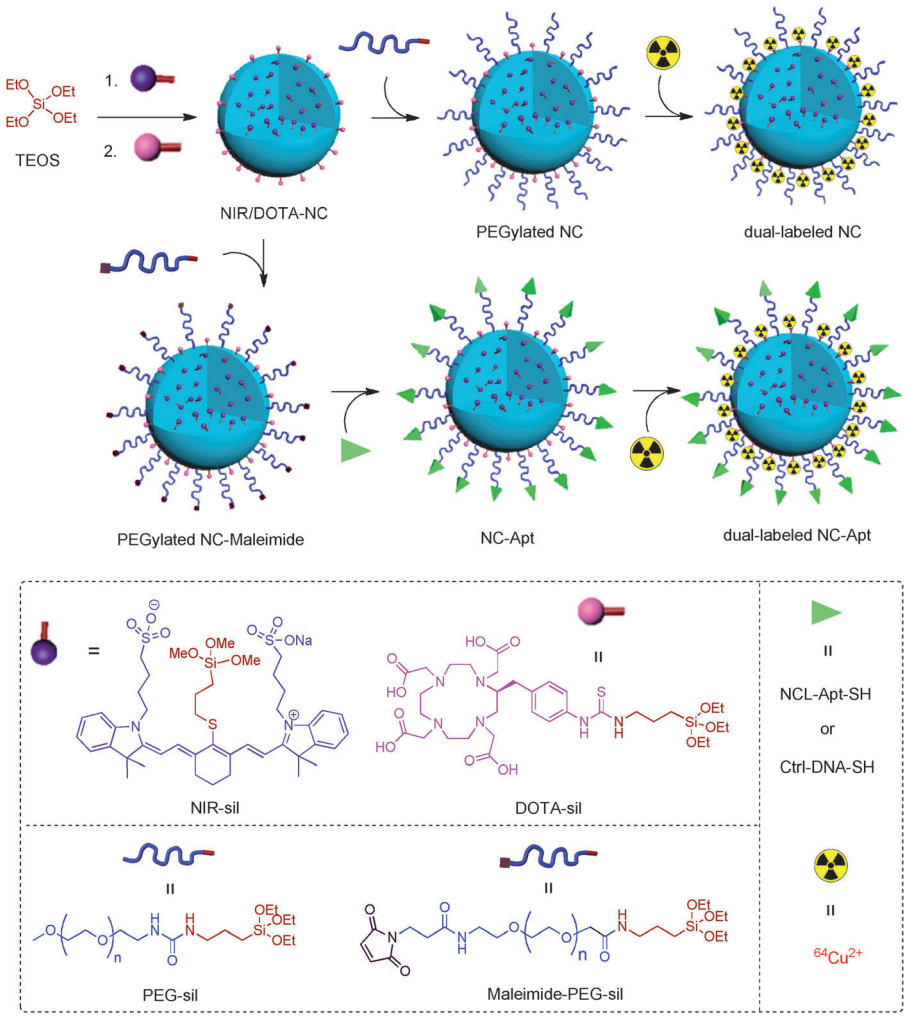

Scheme 1. Preparation of aptamer-functionalized dual-labeled silica NCs for both PET and NIR fluorescence imaging.

We used the described procedure to prepare NIR- and DOTA-modified silica NCs with controlled sizes of 200 nm and 20 nm (denoted NC200 and NC20, respectively; Figure 1a). NC200 and NC20 showed strong fluorescence emission at λ_{em} values of 802.5 nm and 808.0 nm, respectively (Figure 1b).[17] Effective surface modification with DOTA was shown by the ζ-potential measurement (Figure 1c). Both NC200 and NC20 had negatively charged surfaces (−34.8 mV and −136.3 mV, respectively; Figure 1c) at pH 7.4, owing to the surface-bound carboxy groups of DOTA (Scheme 1). These NCs chelated ^{64}Cu cations ($t_{1/2}$ = 12.7 h, β^+ = 17.4 %) with high labeling efficiency (greater than 60 %, Figure 1c and Figure S1) and good stability in 50 % reconstituted human serum (mimicking physiological conditions; Figure S2).

As expected, the size of the as-prepared, dual-modal silica NCs was well controlled.[9] Scanning electron microscopy (SEM) indicated that the diameters of NC200 and NC20 were 198.7 ± 11.8 and 23.1 ± 2.3 nm, respectively (Figure 1a,c). Remarkably narrow size distributions with coefficients of variation (CV), less than 10 %, were observed for both NCs. Thus, these silica NCs, which we designed for preparing multimodal nanoparticulate imaging probes, feature synthetic convenience, flexibility, excellent size control, and modularity that allows for alteration of the functionality and surface chemistry.

To explore the use of the silica NCs for non-invasive PET/CT imaging of LNs in vivo and to identify the optimal NP size for the most efficient LN accumulation, we investigated the lymphatic trafficking of ^{64}Cu-labeled NC200 and NC20 in normal C57BL/6 mice (Figure 2a). Each mouse received small-volume interstitial injections (a commonly used administration route for lymphatic distribution studies)[10f,g,18] of the two NCs, one into each rear hock (left, NC20; right, NC200). PET imaging was carried out to monitor the distribution of the NCs on both sides (Figure 2b). The positions of popliteal LNs (P-LNs), which are the closest LNs to the injection sites, can be clearly identified in the CT images (yellow arrows, Figure 2b). The overlaid CT and PET images show noticeable radioactivity in the left P-LN as early as 12 minutes post injection (p.i.) but not in the right P-LN. The signal increased rapidly in the left P-LN from 3.5 % injected dose per gram of tissue (% I.D. g^{-1}) at 12 minutes p.i. to 9.8 % I.D. g^{-1} at 62 minutes p.i., suggesting fast and efficient lymphatic draining of NC20 (Figure 2d). The amount of accumulated NC20 in the left P-LN continued to increase slightly over time,

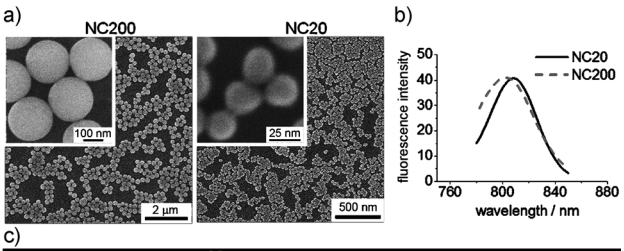

c)

Name of NC	SEM[a] D ± SD (nm)	CV[b] (%)	DNA conjugation C.E.[c] (%)	No. of DNA per NC[d]	ζ-potential (mV)	L.E. of Cu-64[e] (%)
NC200	198.7±11.8	5.94	-	-	-34.8	76.5
NC20	23.1±2.3	9.96	-	-	-36.3	63.1
NC20-Ctrl	22.9±1.9	9.56	73.2	8.6	-41.4	67.6
NC20-Apt	25.1±2.4	8.30	79.6	9.4	-38.3	66.9

Figure 1. a) SEM images of silica NCs. b) Fluorescence emission spectrum of dual-labeled silica NCs. c) Characterization of silica NCs. ([a] Sizes of the hard cores were measured by SEM. D = average diameter, SD = standard deviation. [b] CV = SD/D. [c] Conjugation efficiencies (C.E.) of Ctrl- and Apt-DNA were determined by quantifying the DNA concentration in the supernatant with a Nanodrop spectrophotometer after the NCs were centrifuged down. [d] Number (No.) of DNA molecules per NC was calculated from the DNA/NC feeding ratio and the C.E. value. The silica NC density was set at 2.56 g cm^{-3}. [e] ^{64}Cu labeling efficiency (L.E.) was determined by quantifying the radioactivity in the supernatant with a γ-counter).

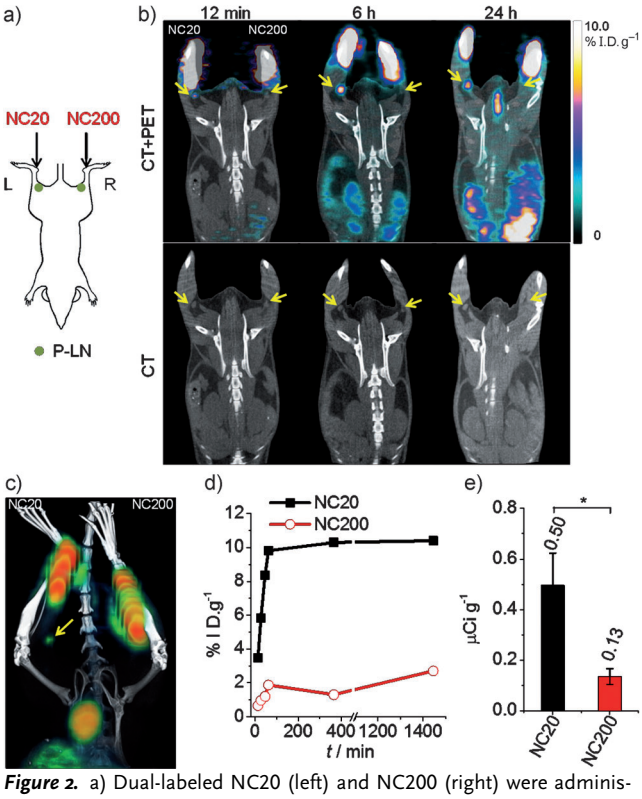

Figure 2. a) Dual-labeled NC20 (left) and NC200 (right) were administered to normal C57BL/6 mice by hock injection; the same amount of radioactivity was injected on each side. b) In vivo whole-body dynamic PET/CT imaging of mice was performed to assess the accumulation of the silica NCs in the P-LNs (yellow arrows). c) Corresponding three-dimensional PET/CT image at 6 h p.i. shows enhanced accumulation of NC20 in the left P-LN (yellow arrow). d) Accumulation of ^{64}Cu-labeled NCs over time in the P-LNs was quantified by selecting the regions of interest in the PET images and analyzing with the instrument software. e) The radioactivity in the excised P-LNs (24 h p.i.) was measured ex vivo with a γ-counter (average ± SD; $n = 3$; * = $p < 0.05$).

eventually reaching a plateau at about six hours p.i. (10.3 % I.D. g^{-1}). This high level of lymphatic accumulation was maintained for as long as 24 hours p.i. (10.4 % I.D. g^{-1}), suggesting that NC20 particles were preferentially retained in the LNs, presumably because they were taken up by phagocytosis by resident nodal macrophages and dendritic cells.[8a,10f,19] In contrast, the signal detected in the right P-LN, on the side that had been injected with NC200, was negligible during the first hour p.i. (0.66 and 1.9 % I.D. g^{-1} at 12 minutes and 62 minutes p.i., respectively); the majority of the NC200 particles remained highly localized at the injection site. The radioactivity in the right P-LN remained low at 6 hours and 24 hours p.i. (1.3 and 2.7 % I.D. g^{-1}, respectively). These observations suggest that NC20 gained entrance to and traveled more easily in the lymphatic system than the NC200. Three-dimensional reconstructed image and movie (Figure 2c, Movie S1) also provide evidence for the significantly enhanced accumulation of NC20 in the left P-LN at 6 hours p.i. At 24 hours p.i., accumulation of NC20 was approximately 3.8 times that of NC200 (Figure 2d). These results were confirmed by *ex vivo* measurement of the radioactivity in the excised P-LNs with a γ-counter (0.50 μCi g^{-1} for NC20 and 0.13 μCi g^{-1} for NC200; Figure 2e).

Because the silica NCs were also labeled with NIR dye, they have the potential to be useful for intraoperative guidance and high-resolution LN imaging. To demonstrate the use of the integrated NIR fluorophore for fluorescence imaging, we harvested the inguinal LNs (I-LNs) from both sides 24 hours p.i. for ex vivo imaging with an Odyssey NIR imaging system (Figure 3a,b). A strong fluorescence signal (298.9) was observed in the left I-LN where NC20 was injected into the ipsilateral hock; whereas a much weaker fluorescence signal (50.5 a.u.) was detected in the right I-LN after injection with NC200 (Figure 3c). The fluorescence enhancement of NC20 in the left I-LN indicates that NC20 migrated approximately six times as efficiently to distant regional LNs through the lymphatic vessels as did NC200.

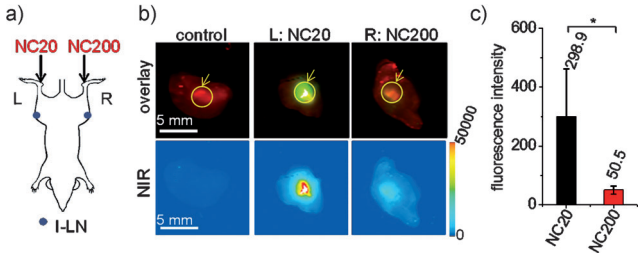

Figure 3. a) Dual-labeled NC20 (left) and NC200 (right) were administered to normal C57BL/6 mice by hock injection. b) I-LNs were collected and imaged for NIR fluorescence at $\lambda_{em} = 800$ nm (green, top) and autofluorescence from tissues (including the surrounding fat) at $\lambda_{em} = 700$ nm (red, top). The I-LNs are indicated by yellow circles and arrows. The bottom row shows the pseudo-colored images of the NIR fluorescence intensity in the I-LNs. c) NIR fluorescence intensity in each I-LN was measured ex vivo at $\lambda_{em} = 800$ nm with an Odyssey NIR imaging system (average ± SD; $n = 3$; * = $p < 0.05$).

The preferential accumulation of NC20 in both the P-LN and the I-LN demonstrates that NC20 was taken up by the lymphatic system much more rapidly and was retained in the LNs at a higher level and for a longer time than their larger counterparts. Because of the sustained LN accumulation, use of NC20 might overcome the problem with vital blue dyes (e.g., Evans blue), which is that they diffuse away from the LNs too rapidly to allow prolonged imaging.[4b,10d] Clearly, the size of the nanoprobes played a vital role in controlling their lymphatic trafficking. NC20 diffused rapidly from the interstitial space into the lymphatic vessels, owing to their small size, and they efficiently migrated to the draining LNs once they reached the lymphatic vessels.[10f,20] NCs with diameters greater than or equal to 100 nm are likely to be internalized by peripheral dendritic cells first and then taken to the LNs by these cells.[10f,20] This process usually takes more than 24 hours, which could explain the small increase in LN accumulation of NC200 at 24 hours p.i. (Figure 2d). Our observations agree with recent reports by Wang et al.[10g] and Reddy et al.[10f] that 20–30 nm NPs are transported to LNs much more efficiently than 100 nm NPs after interstitial injection. The 20 nm NPs may also outperform the 30-50 nm NPs with regard to lymphatic uptake.[10a,e,f,21] In contrast, NPs with sizes less than 8 nm may preferentially migrate to the blood circulation and be cleared rapidly by way of the renal system.[10b,d] Thus, 20 nm silica NCs are likely in the optimum size range (10–20 nm) for the most efficient passive targeting of LNs.

Next, we functionalized the surface of NC20 with NCL-Apts to assess the capability of aptamer-functionalized NCs to target metastatic sentinel LNs. Scheme 1 illustrates the conjugation of NCL-Apt to the surface-bound PEG of silica NCs. Control DNA (Ctrl-DNA) with a random sequence was also conjugated to NC20 for comparison. Conjugation of DNA sequences was achieved with high conjugation efficiency (C.E.; 73.2% for Ctrl-DNA- and 79.6% for NCL-Apt-functionalized NC20s (designated as NC20-Ctrl and NC20-Apt); Figure 1c). The DNA surface densities of NC20-Ctrl and NC20-Apt were on average 8.6 and 9.4 DNA molecules per NC, respectively (Figure 1c).

To evaluate the targeting capability of NC20-Apt in vitro, we separately incubated Rhodamine B isothiocyanate (RITC)-labeled NC20-Ctrl and NC20-Apt with 4T1 murine breast cancer cells. Flow-cytometric analysis showed that there was a 1.6-fold increase in mean fluorescence intensity in 4T1 cells treated with NC20-Apt (20.8 a.u.) versus cells treated with NC20-Ctrl (13.1 a.u.; Figure 4a). Of the cells incubated with NC20-Apt for two hours, 70.7% became fluorescently positive, whereas only 57.5% became positive after incubation with NC20-Ctrl (Figure S3). These results clearly demonstrate that NC20-Apt had the enhanced ability to bind to 4T1 breast cancer cells in vitro.

Because NC20-Apt was selectively taken up by the 4T1 cancer cells, we expected that NC20-Apt would show enhanced accumulation in LNs with metastatic 4T1 tumors. Therefore, we evaluated the capability of NC20-Apt to target metastatic tumors in sentinel LNs in vivo. First, we established an LN metastasis tumor model by hock inoculation of 4T1 cells (stably transfected with firefly luciferase) in both

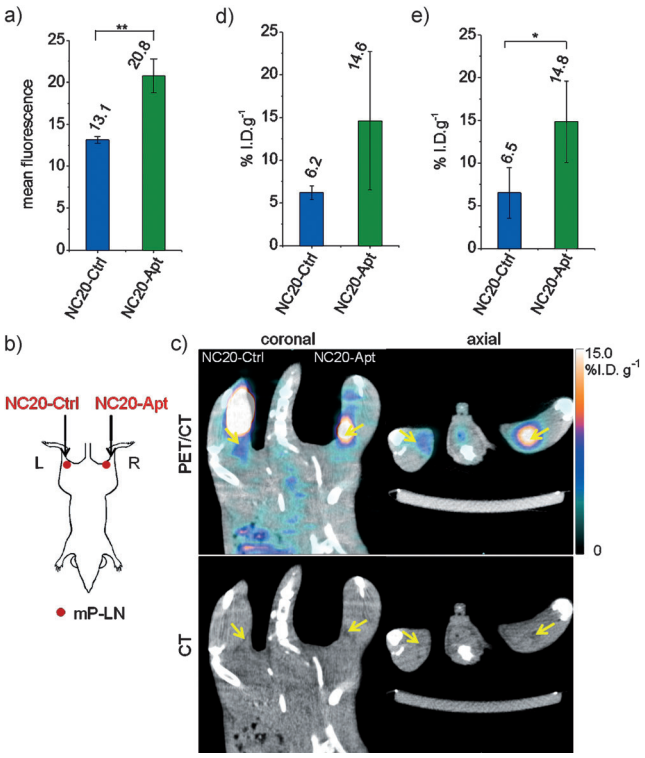

Figure 4. a) In vitro 4T1 cell targeting with NC20-Apt. Internalization of NC20-Ctrl and NC20-Apt by 4T1 cells after 2 h incubation at 37 °C was evaluated from the mean fluorescence of treated cells measured using flow cytometry (** = $p < 0.01$). b) Dual-labeled NC20-Ctrl (left) and NC20-Apt (right) were administered to BALB/c mice with metastatic LNs by hock injection. c) In vivo whole-body PET/CT imaging of BALB/c mice was performed at 24 h p.i. to assess the accumulation of silica NCs in mP-LNs (yellow arrows). d) Accumulation of the ^{64}Cu-labeled NCs in the mP-LNs was quantified by selecting the regions of interest in the PET images and analyzing with the instrument software. e) Accumulation of the ^{64}Cu-labeled NCs was confirmed by ex vivo measurement of excised mP-LNs with a γ-counter (average ± SD; $n = 3$; * = $p < 0.05$).

legs of female BALB/c mice through interstitial injection.[8a,22] After eight days, visible primary tumors had developed, and strong localized bioluminescent signals from 4T1 tumors were detected (Figure S4a). Tumor cells also metastasized to the P-LNs, as evidenced by their enlarged sizes and histological analysis of the excised metastatic P-LNs (mP-LNs, Figure S4b–d).[12c,23] Next, NC20-Ctrl and NC20-Apt were subcutaneously injected into the interstitial space between the primary tumors and the mP-LNs (Figure 4b) in a mouse with mP-LNs on both sides. We acquired PET/CT images 24 hours p.i. to compare the uptake of both NCs in the mP-LNs. A much stronger PET signal was observed in the right mP-LN, on the side injected with NC20-Apt (Figure 4c). The accumulation of NC20-Apt in the mP-LN was approximately 2.3 times that of the NC20-Ctrl, as indicated by quantification of the radioactivity in the PET images (6.2% I.D. g^{-1} for NC20-Ctrl and 14.6% I.D. g^{-1} for NC20-Apt; Figure 4d). This result was also confirmed by ex vivo measurement of the radioactivity in the excised mP-LNs with a γ-counter (6.5% I.D. g^{-1} for NC20-Ctrl and 14.8% I.D. g^{-1} for NC20-Apt; Figure 4e), which correlates well with the in vivo data. In addition, mice

with an mP-LN on one side (right) and a normal P-LN on the other (left) received interstitial injections of NC20-Apt in both rear hocks (Figure S5a). There was an approximately 2.1-fold increase in NC20-Apt accumulation in the mP-LN compared to the normal P-LN (5.9% I.D. g^{-1} for P-LN and 12.1% I.D. g^{-1} for mP-LN; Figure S5b).

The increased accumulation of NC20-Apt in the mP-LNs was likely due to selective uptake by the metastatic 4T1 cells in the mP-LNs.[12a] The enhanced uptake and retention of the aptamer-functionalized dual-modal silica NCs in metastatic LNs permits discrimination of metastatic and normal LNs and thus improves the efficiency of tumor metastasis detection. A widely used strategy for improving accumulation of NPs in LNs is surface decoration of NPs with sugar molecules to enhance uptake by macrophages, which home to the LNs.[24] However, macrophages that take up the sugar-modified NPs may also transport these NPs to the blood, resulting in non-specific accumulation in other organs (e.g., liver and spleen). Antibodies[12b,25] and peptides[8b,12a,c,22] are also employed as active targeting ligands to modify the surface of NPs, to improve the targeting efficiency for metastatic tumors in LNs. However, the application of antibodies or peptides is limited by their relative instability, high cost, and difficult large-scale preparation. Highly specific aptamer-functionalized silica-NC imaging probes may overcome these limitations and have potential applications in the clinic.

In conclusion, we have developed monodisperse, size-controlled silica NCs for dual-modal PET/NIR imaging of sentinel LNs. Dual-modal imaging using this novel probe has unique advantages over conventional lymphatic imaging techniques. For example, PET imaging is a noninvasive diagnostic method and overcomes the depth insensitivity of optical imaging tools, and NIR fluorescence imaging can compensate for the relatively low spatial resolution of PET imaging and potentially provide convenient intraoperative guidance for resection of metastatic LNs once they are identified. When the size of the silica NCs was controlled as 20 nm, they accumulated rapidly and effectively in LNs, thus allowing for improved LN imaging in vivo. For the first time, aptamers were used to functionalize silica NCs for active targeting of lymphatic metastases. Uptake and retention of the aptamer-functionalized silica NCs in metastatic LNs were significantly enhanced compared to the non-targeted silica NCs. These dual-labeled silica NCs hold great potential for improving the accuracy of clinical tumor staging by serving as probes for efficient noninvasive targeted imaging of metastatic LNs.

Received: July 4, 2012
Published online: November 7, 2012

Keywords: aptamers · breast cancer · dual-modal imaging · metastasis targeting · nanoparticles

[1] C. L. Chaffer, R. A. Weinberg, *Science* **2011**, *331*, 1559 – 1564.
[2] T. Tammela, A. Saaristo, T. Holopainen, S. Ylä-Herttuala, L. C. Andersson, S. Virolainen, I. Immonen, K. Alitalo, *Sci. Transl. Med.* **2011**, *3*, 69ra11.
[3] a) T. Aikou, Y. Kitagawa, M. Kitajima, Y. Uenosono, A. J. Bilchik, S. R. Martinez, S. Saha, *Cancer Metastasis Rev.* **2006**, *25*, 269 – 277; b) M. G. Harisinghani, J. Barentsz, P. F. Hahn, W. M. Deserno, S. Tabatabaei, C. H. van de Kaa, J. de La Rosette, R. Weissleder, *N. Engl. J. Med.* **2003**, *348*, 2491 – 2499.
[4] a) R. T. Lucarelli, M. Ogawa, N. Kosaka, B. Turkbey, H. Kobayashi, P. L. Choyke, *Lymphatic Res. Biol.* **2009**, *7*, 205 – 214; b) F. Zhang, G. Niu, G. M. Lu, X. Y. Chen, *Mol. Imaging Biol.* **2011**, *13*, 599 – 612.
[5] a) S. K. Nune, P. Gunda, B. K. Majeti, P. K. Thallapally, M. L. Forrest, *Adv. Drug Delivery Rev.* **2011**, *63*, 876 – 885; b) S. M. Cohen, B. G. Fishinghawk, M. S. Cohen, *Adv. Drug Delivery Rev.* **2011**, *63*, 956 – 962.
[6] S. M. Moghimi, B. Bonnemain, *Adv. Drug Delivery Rev.* **1999**, *37*, 295 – 312.
[7] Y. Sun, M. X. Yu, S. Liang, Y. J. Zhang, C. G. Li, T. T. Mou, W. J. Yang, X. Z. Zhang, B. A. Li, C. H. Huang, F. Y. Li, *Biomaterials* **2011**, *32*, 2999 – 3007.
[8] a) X. L. Huang, F. Zhang, S. Lee, M. Swierczewska, D. O. Kiesewetter, L. X. Lang, G. F. Zhang, L. Zhu, H. K. Gao, H. S. Choi, G. Niu, X. Y. Chen, *Biomaterials* **2012**, *33*, 4370 – 4378; b) M. Benezra, O. Penate-Medina, P. B. Zanzonico, D. Schaer, H. Ow, A. Burns, E. DeStanchina, V. Longo, E. Herz, S. Iyer, J. Wolchok, S. M. Larson, U. Wiesner, M. S. Bradbury, *J. Clin. Invest.* **2011**, *121*, 2768 – 2780; c) R. Kumar, I. Roy, T. Y. Ohulchanskky, L. A. Vathy, E. J. Bergey, M. Sajjad, P. N. Prasad, *ACS Nano* **2010**, *4*, 699 – 708; d) L. Wang, K. M. Wang, S. Santra, X. J. Zhao, L. R. Hilliard, J. E. Smith, J. R. Wu, W. H. Tan, *Anal. Chem.* **2006**, *78*, 646 – 654; e) W. J. Rieter, J. S. Kim, K. M. L. Taylor, H. Y. An, W. L. Lin, T. Tarrant, W. B. Lin, *Angew. Chem.* **2007**, *119*, 3754 – 3756; *Angew. Chem. Int. Ed.* **2007**, *46*, 3680 – 3682; f) H. Meng, M. Xue, T. Xia, Z. Ji, D. Y. Tarn, J. I. Zink, A. E. Nel, *ACS Nano* **2011**, *5*, 4131 – 4144.
[9] L. Tang, T. M. Fan, L. B. Borst, J. Cheng, *ACS Nano* **2012**, *6*, 3954 – 3966.
[10] a) X. Cai, W. Li, C.-H. Kim, Y. Yuan, L. V. Wang, Y. Xia, *ACS Nano* **2011**, *5*, 9658 – 9667; b) L. M. Kaminskas, C. J. H. Porter, *Adv. Drug Delivery Rev.* **2011**, *63*, 890 – 900; c) C. Oussoren, G. Storm, *Adv. Drug Delivery Rev.* **2001**, *50*, 143 – 156; d) H. Kobayashi, S. Kawamoto, M. Bernardo, M. W. Brechbiel, M. V. Knopp, P. L. Choyke, *J. Controlled Release* **2006**, *111*, 343 – 351; e) S. T. Reddy, A. Rehor, H. G. Schmoekel, J. A. Hubbell, M. A. Swartz, *J. Controlled Release* **2006**, *112*, 26 – 34; f) S. T. Reddy, A. J. van der Vlies, E. Simeoni, V. Angeli, G. J. Randolph, C. P. O'Neil, L. K. Lee, M. A. Swartz, J. A. Hubbell, *Nat. Biotechnol.* **2007**, *25*, 1159 – 1164; g) H. Wang, S. T. Wang, H. Su, K. J. Chen, A. L. Armijo, W. Y. Lin, Y. J. Wang, J. Sun, K. Kamei, J. Czernin, C. G. Radu, H. R. Tseng, *Angew. Chem.* **2009**, *121*, 4408 – 4412; *Angew. Chem. Int. Ed.* **2009**, *48*, 4344 – 4348; h) T. T. Goodman, P. L. Olive, S. H. Pun, *Int. J. Nanomed.* **2007**, *2*, 265 – 274; i) S. D. Perrault, C. Walkey, T. Jennings, H. C. Fischer, W. C. W. Chan, *Nano Lett.* **2009**, *9*, 1909 – 1915.
[11] a) D. Peer, J. M. Karp, S. Hong, O. C. Farokhzad, R. Margalit, R. Langer, *Nat. Nanotechnol.* **2007**, *2*, 751 – 760; b) M. E. Davis, Z. Chen, D. M. Shin, *Nat. Rev. Drug Discovery* **2008**, *7*, 771 – 782.
[12] a) C. Leuschner, C. Kumar, W. Hansel, W. Soboyejo, J. K. Zhou, J. Hormes, *Breast Cancer Res. Treat.* **2006**, *99*, 163 – 176; b) L. Sampath, S. Kwon, M. A. Hall, R. E. Price, E. M. Sevick-Muraca, *Transl. Oncol.* **2010**, *3*, 307 – 317; c) Z. Q. Yan, C. Y. Zhan, Z. Y. Wen, L. L. Feng, F. Wang, Y. Liu, X. K. Yang, Q. Dong, M. Liu, W. Y. Lu, *Nanotechnology* **2011**, *22*, 415103.
[13] a) D. Shangguan, Y. Li, Z. W. Tang, Z. H. C. Cao, H. W. Chen, P. Mallikaratchy, K. Sefah, C. Y. J. Yang, W. H. Tan, *Proc. Natl. Acad. Sci. USA* **2006**, *103*, 11838 – 11843; b) J. Cheng, B. A. Teply, I. Sherifi, J. Sung, G. Luther, F. X. Gu, E. Levy-Nissenbaum, A. F. Radovic-Moreno, R. Langer, O. C. Farokhzad, *Biomaterials* **2007**, *28*, 869 – 876; c) O. C. Farokhzad, J.

Cheng, B. A. Teply, I. Sherifi, S. Jon, P. W. Kantoff, J. P. Richie, R. Langer, *Proc. Natl. Acad. Sci. USA* **2006**, *103*, 6315 – 6320.
[14] a) Z. Cao, R. Tong, A. Mishra, W. Xu, G. C. L. Wong, J. Cheng, Y. Lu, *Angew. Chem.* **2009**, *121*, 6616 – 6620; *Angew. Chem. Int. Ed.* **2009**, *48*, 6494 – 6498; b) S. Christian, J. Pilch, M. E. Akerman, K. Porkka, P. Laakkonen, E. Ruoslahti, *J. Cell Biol.* **2003**, *163*, 871 – 878; c) S. Soundararajan, W. W. Chen, E. K. Spicer, N. Courtenay-Luck, D. J. Fernandes, *Cancer Res.* **2008**, *68*, 2358 – 2365.
[15] S. W. Ha, C. E. Camalier, G. R. Beck, J. K. Lee, *Chem. Commun.* **2009**, 2881 – 2883.
[16] P. Caliceti, F. M. Veronese, *Adv. Drug Delivery Rev.* **2003**, *55*, 1261 – 1277.
[17] N. Narayanan, G. Patonay, *J. Org. Chem.* **1995**, *60*, 2391 – 2395.
[18] E. J. Chaney, L. Tang, R. Tong, J. J. Cheng, S. A. Boppart, *Mol. Imaging* **2010**, *9*, 153 – 162.
[19] J. C. Alex, D. L. Weaver, J. T. Fairbank, B. S. Rankin, D. N. Krag, *Surg. Oncol.* **1993**, *2*, 303 – 308.
[20] M. F. Bachmann, G. T. Jennings, *Nat. Rev. Immunol.* **2010**, *10*, 787 – 796.
[21] S. M. Moghimi, A. C. Hunter, J. C. Murray, *FASEB J.* **2005**, *19*, 311 – 330.
[22] F. Zhang, G. Niu, X. Lin, O. Jacobson, Y. Ma, H. Eden, Y. He, G. Lu, X. Chen, *Amino Acids* **2012**, *42*, 2343 – 2351.
[23] Z. Q. Yan, F. Wang, Z. Y. Wen, C. Y. Zhan, L. L. Feng, Y. Liu, X. L. Wei, C. Xie, W. Y. Lu, *J. Controlled Release* **2012**, *157*, 118 – 125.
[24] a) V. Q. Hieu, M. K. Yoo, H. J. Jeong, H. J. Lee, M. Muthiah, J. H. Rhee, J. H. Lee, C. S. Cho, Y. Y. Jeong, I. K. Park, *Acta Biomater.* **2011**, *7*, 3935 – 3945; b) B. E. Ocampo-García, F. d. M. Ramírez, G. Ferro-Flores, L. M. De León-Rodríguez, C. L. Santos-Cuevas, E. Morales-Avila, C. Arteaga de Murphy, M. Pedraza-López, L. A. Medina, M. A. Camacho-López, *Nucl. Med. Biol.* **2011**, *38*, 1 – 11.
[25] M. Takeda, H. Tada, H. Higuchi, Y. Kobayashi, M. Kobayashi, Y. Sakurai, T. Ishida, N. Ohuchi, *Breast Cancer* **2008**, *15*, 145 – 152.

